Modulation of Attosecond Beating in Resonant Two-Photon Ionization

Álvaro Jiménez-Galán,[1] Luca Argenti,[1,*] and Fernando Martín[1,2]
[1]Departamento de Química, Módulo 13, Universidad Autónoma de Madrid, 28049 Madrid, Spain, EU
[2]Instituto Madrileño de Estudios Avanzados en Nanociencia (IMDEA-Nanociencia), Cantoblanco 28049 Madrid, Spain, EU

(Received 19 May 2014; published 24 December 2014)

We present a theoretical study of the photoelectron attosecond beating due to interference of two-photon transitions in the presence of autoionizing states. We show that, as a harmonic traverses a resonance, both the phase shift and frequency of the sideband beating significantly vary with photon energy. Furthermore, the beating between two resonant paths persists even when the pump and the probe pulses do not overlap, thus providing a nonholographic interferometric means to reconstruct coherent metastable wave packets. We characterize these phenomena by means of a general analytical model that accounts for the effect of both intermediate and final resonances on two-photon processes. The model predictions are in excellent agreement with those of accurate *ab initio* calculations for the helium atom in the region of the $N = 2$ doubly excited states.

DOI: 10.1103/PhysRevLett.113.263001 PACS numbers: 32.80.Qk, 32.80.Fb, 32.80.Rm, 32.80.Zb

Attosecond experiments [1–3] can provide a time-resolved view [4] of the ultrafast electron dynamics that occurs in atoms and molecules (see, e.g., Refs. [5–7]). A popular approach is the technique of reconstruction of attosecond beating by interference of two-photon transitions (RABBIT) [8]. In this technique, a pump extreme-ultraviolet attosecond-pulse train (XUV-APT) is used in association with a compressed infrared (IR) probe pulse to ionize the target atom or molecule, and the photoelectron spectrum is recorded as a function of the pump-probe time delay, τ. In the long-pulse limit, the APT only contains photons of frequencies $\omega_{\mathrm{H}_{2n+1}}$, which are odd multiples H_{2n+1} of the IR carrier frequency ω_{IR}. Thus, the transition amplitudes for the two paths leading to the same photoelectron energy, $\mathrm{A} + \hbar\omega_{\mathrm{H}_{2n\pm1}} \mp \hbar\omega_{\mathrm{IR}} \rightarrow \mathrm{A}^+ + e^-$, interfere, giving rise to a sideband SB_{2n} whose intensity oscillates as a function of τ with frequency $2\omega_{\mathrm{IR}}$ and phase shift φ_{2n} given by the relative phase between the two consecutive $H_{2n\pm1}$ harmonics and the so-called relative atomic phase [9]: $\Delta I_{2n} \sim \cos(2\omega_{\mathrm{IR}}\tau + \varphi_{2n})$. The RABBIT technique, therefore, can be used to reconstruct either the APT from the harmonic phases [10], if the atomic phases are known, or the atomic phases [11–13], if the APT shape is known.

An appealing perspective is to use attosecond technologies to investigate photoionization processes governed by electron correlation [14–17]. In particular, correlation is responsible for the Auger (or autoionization) decay of multiply-excited states, a resonant process that may require several tens of femtoseconds to complete. Consequently, as for bound states [18–22], the presence of autoionizing states, either as intermediate or final states, can dramatically alter the atomic photoionization spectra [23–35]. RABBIT has been used to investigate resonant processes in which the contribution of the direct-ionization amplitude is negligible, namely, when bound electronic states are directly excited by the XUV-APT (as in helium [19]) or when autoionizing vibronic states are populated by the XUV-APT without simultaneous excitation of the ionization continuum (as in the N_2 molecule [36]). These RABBIT experiments [19,36] are compatible with a jump of π in the sideband phase shift, as the energy of one of the adjacent harmonics traverses the resonant intermediate state. To our knowledge, RABBIT has never been used when both nonresonant continuum and resonant amplitudes contribute to the total ionization amplitude in similar amounts, a circumstance that is the rule more than the exception, e.g., when atomic doubly excited states (DES) are populated from the ground state. Furthermore, the lifetimes of autoionizing resonances are often comparable to or larger than the duration of the ultrashort pulses employed in common attosecond pump-probe schemes. As a consequence, even in perturbative conditions, a stationary regime is never achieved and the stationary models used to extract dynamical information from RABBIT are outright inapplicable. All the above leads to obvious complications in the analysis of the RABBIT spectrum.

In this Letter, we theoretically analyze the effect of intermediate and final autoionizing states on the RABBIT photoelectron spectrum of He. To do so, we have solved the full dimensional time-dependent Schrödinger equation (TDSE) by using a nearly exact method [9,30,37] and interpreted these results in terms of an analytical time-resolved model, based on Fano's autoionization theory [38], which, from a minimum set of parameters, is able to reproduce with high accuracy the *ab initio* photoelectron spectrum for arbitrary pulses. We focus, in particular, on He DES lying below the $N = 2$ excitation threshold of the

He^+ parent ion [39–41]. Our results show that, when intermediate autoionizing states are involved, the RABBIT photoelectron spectra do not follow the existing picture. First, as a consequence of the finite pulse duration, the frequency of the sideband oscillation is no longer $2\omega_{IR}$, and it displays a pronounced resonant modulation. Second, as a consequence of the interplay between the resonant and nonresonant contributions, the local phase shift does not undergo a π excursion anymore. Finally, RABBIT oscillations persist even when the time delay is so large that the probe pulse does not overlap with the APT anymore. The local beating phase can then be used to reconstruct the coherent metastable wave packet created by the pump pulse.

Figure 1 shows a representative example of *ab initio* results based on the solution of the TDSE for the helium atom ionized from the ground state with an XUV-APT in conjunction with a weak 845-nm IR pulse. Figure 2 (top) shows the SB_{38-42} sidebands that arise when the sp_2^+ DES is resonantly excited by the H_{41} harmonic ($\hbar\omega_{IR} = 1.466$ eV). The peak intensity and the full width at half maximum (FWHM) of the APT are $I_{APT} = 5$ GW/cm^2 and

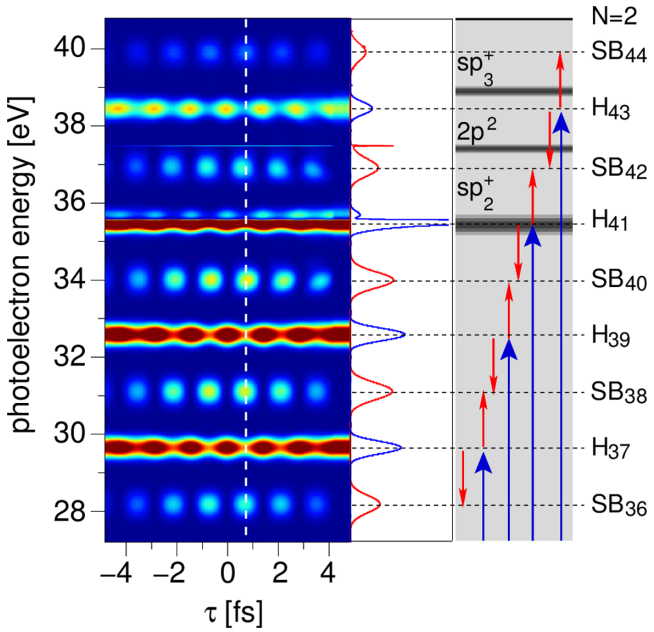

FIG. 1 (color online). Left panel: The *ab initio* photoelectron spectrum for the XUV-APT-pump weak-IR-probe ionization of He in the region of the $N = 2$ DESs as a function of pump-probe time delay. The APT is centered at $\hbar\omega_{APT} = 57.21$ eV ($IP_{He} = 24.6$ eV), with fundamental frequency $\hbar\omega_{IR} = 1.466$ eV; both the pump and the probe have FWHM of about 7 fs. Central panel: Signal at a fixed time delay (white dashed line). Right panel: Outline of the relevant states in the process. Starting from the $1s^2$ ground state, the atom absorbs a XUV photon from the APT and exchanges an IR photon with the probe pulse, leading to strong H_{2n+1} harmonic signals in the $^1P^o$ continuum and to weak SB_{2n} sideband signals in the $^1S^e$ and $^1D^e$ continua.

$FWHM_{APT} = 6.8$ fs, and those of the IR-probe pulse are $I_{IR} = 10$ GW/cm^2 and $FWHM_{IR} = 7.2$ fs. One can clearly see a local phase shift of the sidebands that increases approximately linearly in a wide time-delay interval. Stated otherwise, the resonance alters the RABBIT beating *frequency* itself.

To understand this behavior, we have developed a model in which the standard formulation of second-order perturbation theory is extended to account for the finite duration of the pulse. In this model, the transition amplitude between an initial state i of energy E_i and a final state f of energy E_f is (atomic units are used unless otherwise stated)

$$\mathcal{A}^{(2)}_{f\leftarrow i} = -i\int_{-\infty}^{\infty} d\omega \tilde{A}_{IR}(\omega_{fi}-\omega)\tilde{A}_{APT}(\omega)\mathcal{M}_{fi}(\omega), \quad (1)$$

where

$$\mathcal{M}_{fi}(\omega) = \alpha^2\langle\psi_f|P_z G_0^+(E_i+\omega)P_z|\psi_i\rangle \quad (2)$$

is the usual monochromatic two-photon transition amplitude in velocity gauge, $\omega_{fi} = E_f - E_i$, α is the fine-structure constant, $G_0^+(E) = (E - H + i0^+)^{-1}$ is the retarded resolvent of the field-free Hamiltonian, P_z is the electron momentum operator, and $\tilde{A}_{IR,APT}(\omega) = (2\pi)^{-1/2}\int dt A_{IR,APT}(t)\exp(i\omega t)$ are the Fourier transforms of the vector potentials along the polarization axis. The $\mathcal{A}^{(2)}_{f\leftarrow i}$ amplitude includes two contributions, $\mathcal{A}^+$ and $\mathcal{A}^-$, which correspond to the absorption of an XUV photon from the $H_{2n\pm1}$ harmonic followed by the coherent emission or absorption of an IR photon. The intensity of the sideband is given by the square module of the total amplitude,

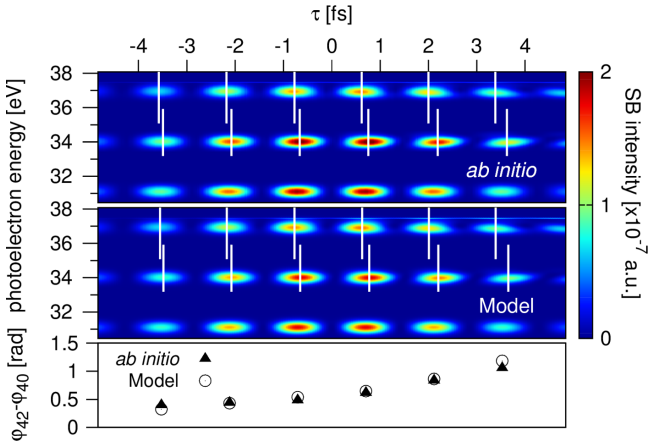

FIG. 2 (color online). Calculated spectrum of the SB_{38}, SB_{40}, and SB_{42} sidebands, as a function of pump-probe time delay, for the fixed carrier energy $\hbar\omega_{IR} = 1.466$ eV. Top panel: The *ab initio* results. Central panel: Results from the model (see text). Bottom panel: Difference between the position of the maxima in sidebands SB_{42} and SB_{40}. The SB_{42} beating *frequency* is higher than for SB_{40} due to the resonant excitation of the sp_2^+ DES by the H_{41} harmonic.

$$I_{\mathrm{SB}}(\tau) = |\mathcal{A}^{+}(\tau)|^2 + |\mathcal{A}^{-}(\tau)|^2 + 2\Re e[\mathcal{A}^{+*}(\tau)\mathcal{A}^{-}(\tau)]. \tag{3}$$

The local phase $\varphi(\omega_{\mathrm{IR}}, \tau)$ of the sideband modulation is the argument of the complex interference term $\mathcal{A}^{+*}(\tau)\mathcal{A}^{-}(\tau)$, and it can be decomposed in the usual phase $2\omega_{\mathrm{IR}}\tau$ plus an additional dephasing $\varphi_{2n}(\omega_{\mathrm{IR}}, \tau)$ that, in general, depends on both frequency of the laser and time delay.

In the absence of intermediate and final autoionizing states, which is the usual scenario for RABBIT spectroscopy, and for electron energies much larger than ω_{IR}, the two amplitudes take on the form

$$\mathcal{A}^{\pm} = \mathcal{F}(\tau) e^{\mp i\omega_{\mathrm{IR}}\tau} w(z^{\pm}_{\mathrm{dir}}), \tag{4}$$

where $\mathcal{F}(\tau)$ is a factor common to both $\mathcal{A}^{\pm}$ amplitudes [42], $w(z)$ is the special function $\exp(-z^2)[1 - \mathrm{erf}(-iz)]$ [43], $z^{\pm}_{\mathrm{dir}} = \sigma_t(\omega^{\pm} - \omega_{fi})/\sqrt{2}$, σ_t is the time interval in which the pump and probe pulses overlap, and $\omega^{\pm} = \omega_{\mathrm{H}_{2n\pm1}} + [(\omega_{fi} - 2n\omega_{\mathrm{IR}})/\sigma^2_{\mathrm{IR}} - i\tau]/\sigma^2_t$. Equation (4) is the generalization of the known expression for cw light [44] to Gaussian pulses.

Here, we are interested in analyzing how the usual appearance of the nonresonant RABBIT spectra described by Eq. (4) (or its equivalent monochromatic version of Ref. [44]) is modified when autoionizing states are populated. To do so, we follow the standard Fano approach [38] and express the continuum states as

$$|\psi_E\rangle = |E\rangle + \left(\int d\varepsilon |\varepsilon\rangle \frac{V_{\varepsilon a}}{E - \varepsilon + i0^+} + |a\rangle \right) \frac{V_{aE}}{E - \tilde{E}_a}, \tag{5}$$

where $|E\rangle$ is the nonresonant continuum leading to the nonresonant amplitudes (4), $|a\rangle$ is the localized part of an isolated autoionizing state of energy $E_a + \Delta_a$ (Δ_a is the so-called energy shift [38]) and autoionization width $\Gamma_a = 2\pi|V_{aE_a}|^2$, $\tilde{E}_a$ is the complex resonance energy $\tilde{E}_a = E_a + \Delta_a - i\Gamma_a/2$, V_{nm} is the Hamiltonian coupling between states n and m, and the integral within the parentheses is the so-called modified continuum. To simplify the notation, we have only considered a single autoionizing state $|a\rangle$ and a single ionization channel.

From Eq. (5), the transition amplitude (2) for the case of a single intermediate autoionizing state can be written as the sum of a slowly varying direct-ionization component $\mathcal{M}^{\mathrm{dir}}_{fi}$ and a resonant component $\mathcal{M}^{\mathrm{res}}_{fi} \propto (\omega_{\mathrm{H}_{2n\pm1}} - \omega_{\tilde{a}i})^{-1}$, where $\omega_{\tilde{a}i} = \tilde{E}_a - E_i$. As the harmonic frequency $\omega_{\mathrm{H}_{2n\pm1}}$ traverses the resonance, the $\mathcal{M}_{fi}$ amplitude describes a circle in the complex plane. If $\mathcal{M}^{\mathrm{dir}}_{fi}$ is negligible, the circle starts and ends at the origin, and its phase increases by π in going from below to above E_a [Fig. 3(a)]. In the more common case of a non-negligible $\mathcal{M}^{\mathrm{dir}}_{fi}$, the circle is shifted with respect to the origin [Fig. 3(b)] and, consequently, its phase changes as one traverses E_a but goes back to its initial value. For finite pulses, the convolution with their spectral function in Eq. (1) contracts the circle, thus reducing the phase variation [Fig. 3(c)]. The corresponding $\mathcal{A}^{\pm}$ amplitudes are

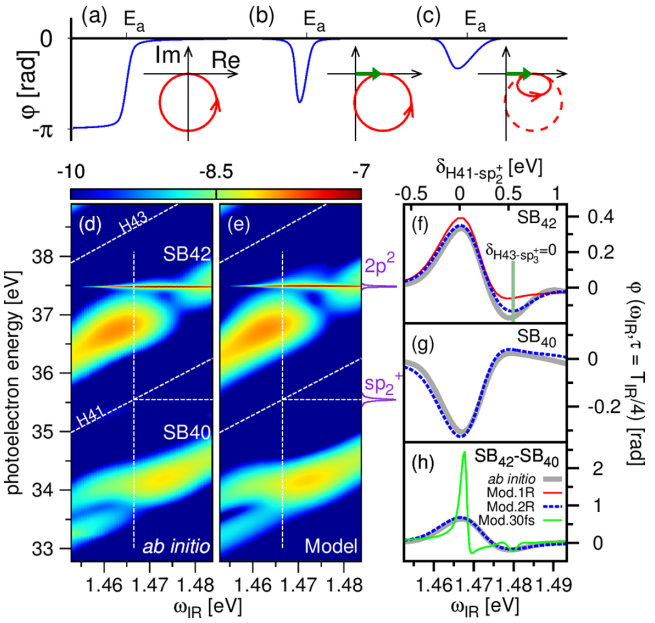

FIG. 3 (color online). Top panel: Sketch of the transition amplitude in the complex plane and its phase profile for (a) $\mathcal{M}^{\mathrm{dir}}_{fi} = 0$, (b) $\mathcal{M}^{\mathrm{dir}}_{fi} \neq 0$, (c) $\mathcal{M}^{\mathrm{dir}}_{fi} \neq 0$ and finite pulse duration (see text). On the bottom left: Sidebands SB_{40} and SB_{42} vs ω_{IR}, for $\tau = 0$, computed (d) *ab initio* and (e) with the model. (f–h): Comparison of the phase shifts, in the $[0, T_{\mathrm{IR}}/2]$ time-delay interval, of the energy-integrated signals. The gray thick solid line is the *ab initio* calculation, the red solid line and blue dashed line are the model prediction with one and two intermediate resonances, respectively ($\mathrm{FWHM}_{\mathrm{IR}} = 7.2$ fs, $\mathrm{FWHM}_{\mathrm{APT}} = 6.8$ fs), and the green solid line is the model prediction for $\mathrm{FWHM}_{\mathrm{IR}} = 30$ fs and $\mathrm{FWHM}_{\mathrm{APT}} = 10$ fs. The sp_2^+ resonance gives rise to a large peak in the dephasing between the two sidebands.

$$\mathcal{A}^{\pm} = \mathcal{F}(\tau) e^{\mp i\omega_{\mathrm{IR}}\tau} [w(z^{\pm}_{\mathrm{dir}}) + (\beta_{fa} - \epsilon^{-1}_{fa})(q'_a - i) w(z^{\pm}_a)], \tag{6}$$

where, in addition to the nonresonant contribution given in Eq. (4), one can immediately recognize an additional term due to the presence of the autoionizing state a. In this term, $z^{\pm}_a = \sigma_t(\omega^{\pm} - \omega_{\tilde{a}i})/\sqrt{2}$ and $\epsilon_{fa} = 2\omega_{fa}/\Gamma_a$ is the reduced energy as defined by Fano [38]. The parameters in the resonant part of the amplitude measure the relative strength of different transitions: from the ground state to the resonance vs to the intermediate continuum ($q'_a = \mathcal{O}_{ia}/\pi V_{Ea}\mathcal{O}_{iE}$) and to the final state from the resonance vs from the intermediate continuum ($\beta_{fa} = \pi\mathcal{O}_{fa}|V_{aE}|/\int dE' \mathcal{O}_{E_f E'}$). Here, $\mathcal{O}_{mn}$ is the generic dipole-transition integral $\langle\psi_m|P_z|\psi_n\rangle$.

From the expression of the $\mathcal{A}^{\pm}$ amplitudes given in Eq. (6), it is a simple task to derive the sideband phase $\varphi_{2n}(\omega_{\mathrm{IR}},\tau)$ as a function of the minimal set of resonant atomic parameters. Conversely, these parameters can be determined by comparing the model predictions with a few selected experiments [42]. We applied this latter procedure to He by using our nearly exact *ab initio* solutions of the TDSE [9,30,37] as "numerical experiments."

Figure 2 (central panel) shows the results obtained with our model. The agreement with the *ab initio* results is excellent. The population of the sp_2^+ state by H_{41} results in a sideband frequency modulation of $\delta\omega = -0.073$ eV, which is obtained by Fourier analyzing the energy-integrated sideband signal. This value is nearly the same as that obtained from the *ab initio* calculations (Fig. 2, top panel). It is important to stress that, in the absence of intermediate resonances, the finite duration of the pulses already induces a redshift of $\delta\omega = -0.038$ eV, due to the fact that the nonresonant component $\mathcal{M}_{fi}^{\mathrm{dir}}$ is inversely proportional to the energy of the last exchanged IR photon, thus amplifying the low-frequency components in the beating. Removing this nonresonant detuning, the frequency modulation due to the sp_2^+ resonance is -0.035 eV, i.e., 1.2% of $2\omega_{\mathrm{IR}}$, which corresponds to a change in the RABBIT period of 17 as. To a good approximation, the frequency detuning is nearly independent of τ; i.e., the phase shift φ_{2n} is well described by its first-order approximation $\varphi_{2n}(\omega_{\mathrm{IR}},\tau) = \varphi_{2n}^0(\omega_{\mathrm{IR}}) + \delta\omega(\omega_{\mathrm{IR}})\tau$ (Fig. 2, bottom panel).

Figures 3(d) and 3(e) show the energy-resolved SB_{40} and SB_{42} sidebands, computed either *ab initio* or with the model, as a function of the IR photon energy [equivalent to the harmonic-DES detuning, $\delta_{H_{2n+1}-a} = (2n+1)\omega_{\mathrm{IR}} - \omega_{ai}$] for a fixed time delay, $\tau = 0$, close to the minimum of the beating. In this case, the model included the two bright $sp_{2/3}^+$ intermediate $^1P^o$ resonances as well as the final ^1S $2p^2$ resonance. These two plots illustrate well two aspects of the effects of resonances in RABBIT experiments. First, while the upper sideband displays a maximum at negative and a minimum at positive detuning of the H_{41} resonant harmonic energy with respect to the excitation energy of the sp_2^+ state from the ground state, the opposite is true for the lower sideband. Second, due to the strong $sp_2^+ - 2p^2$ coupling, the $2p^2$ state already starts populating when the sp_2^+ state is resonant with the H_{41} harmonic ($\hbar\omega_{\mathrm{IR}} = 1.466$ eV), i.e., well before the $2p^2$ state is resonant with the SB_{42} sideband ($\hbar\omega_{\mathrm{IR}} = 1.478$ eV).

These aspects are reflected in the sideband phase shift vs resonance-detuning plots shown in Figs. 3(f)–3(h). The phase profile is clearly very different from a π jump, and it becomes even more pronounced when longer pulses are used (30 fs). In either case, the dephasing is sufficiently large (0.8 and 2.5 rad) to be experimentally observable [45]. The signature of the upper sp_3^+ DES, which is resonant at $\hbar\omega_{\mathrm{IR}} = 1.48$ eV, is recognizable in Fig. 3(f).

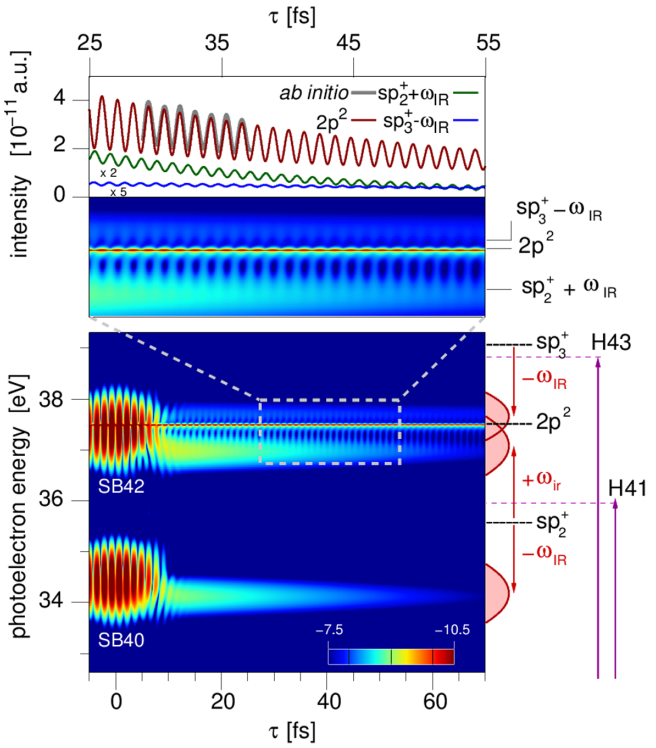

FIG. 4 (color online). Bottom panel: Spectrum of the $SB_{40,42}$ sidebands vs τ computed with the model, for $\hbar\omega_{\mathrm{IR}} = 1.475$ eV. The harmonics H_{41} and H_{43} (not shown) are detuned from the sp_2^+ and sp_3^+ $^1P^o$ DES by $\delta_{H_{41}-sp_2^+} = 0.37$ eV and $\delta_{H_{43}-sp_3^+} = -0.19$ eV, respectively. Top panel: The modeled final $2p^2$ resonant signal (red solid line), which dominates the spectrum, reproduces the *ab initio* prediction (gray thick solid line) with high accuracy.

Indeed, inclusion of the sp_3^+ state brings the model into much better agreement with the simulation.

Figure 4 shows the $SB_{40,42}$ sidebands in a wide range of time delays for $\omega_{\mathrm{IR}} = 1.475$ eV. When the APT and the IR pulse overlap ($|\tau| \lesssim 5$ fs), the sidebands are dominated by the nonresonant signal and are centered at $E = 2n\omega_{\mathrm{IR}} - \mathrm{IP}$, where IP is the ionization potential. Between 5 fs and 10 fs, the nonresonant contributions disappear, while the sidebands narrow and shift to symmetric positions around the two resonances. In contrast with nonresonant two-photon transitions, the sideband signals persist even when the pump and the probe do not overlap. Furthermore, the SB_{42} sideband displays the characteristic interference fringes of the $sp_2^+ - sp_3^+$ beating, with a lifetime intermediate between those of the two resonances. The strongest contribution to the sideband comes from the transition to the $2p^2$ state, which is permitted even at the level of the independent-particle approximation. The q parameters for the excitation of the $2p^2$ state from either the sp_2^+ or the sp_3^+ state differ, thus giving rise to an oscillating effective $q_{\mathrm{eff}}(\tau)$ that manifests as a beating of the background continuum out of phase with respect to that of the final

resonance. This beating could be used to reconstruct the autoionizing wave packet, following concepts similar to those based on the holographic principle [46].

In conclusion, we have solved the TDSE and developed an analytical model for the two-photon ionization of atoms with finite pulses, in the presence of autoionizing states. The model shows that both the contribution of intermediate continuum states and the finite duration of the light pulses must be taken into account to achieve qualitatively correct interpretations of resonant attosecond pump-probe experiments. In particular, we have demonstrated that (i) intermediate resonances manifest themselves in RABBIT experiments with variations in the sideband phase shift and beating frequency as a function of the fundamental carrier frequency, and (ii) resonances in the final states appear in the photoelectron spectrum as Fano-like profiles, strongly modulated with respect to the pump-probe time delay and out of phase with respect to the background signal. For the realistic cases we have examined, the variation of the sideband phase shift should be detectable with current instrumental resolution. Despite its simplicity, the model is able to provide results in quantitative agreement with accurate *ab initio* solutions of the TDSE, thus permitting us to explore a vast range of pulse parameters at a negligible computational cost or, conversely, to extract radiative-transition strengths between multiply-excited states, which are hard to obtain otherwise. In addition, we have found that long-lived resonances excited by consecutive harmonics give rise to sideband beatings that persist even when the pump and probe pulses do not overlap and from which the coherent metastable wave packet can be reconstructed. These conclusions remain valid when non-Fourier-limited pulses or XUV frequencies that are not strictly multiples of the IR frequency are used [42].

We thank Richard Taïeb, Alfred Maquet, Jeremie Caillat, and Pascal Salières for useful discussions and their kind hospitality. We acknowledge computer time from the CCC-UAM and Marenostrum Supercomputer Centers and financial support from the European Research Council under the European Union's Seventh Framework Programme (FP7/2007-2013)/ERC Grant Agreement No. 290853 XCHEM, the MINECO Project No. FIS2013-42002-R, the ERA-Chemistry Project No. PIM2010EEC-00751, and the European COST Action XLIC CM1204.

*luca.argenti@uam.es

[1] F. Krausz and M. Y. Ivanov, Rev. Mod. Phys. **81**, 163 (2009).
[2] T. Popmintchev, M.-C. Chen, P. Arpin, M. M. Murnane, and H. C. Kapteyn, Nat. Photonics **4**, 822 (2010).
[3] G. Sansone, L. Poletto, and M. Nisoli, Nat. Photonics **5**, 655 (2011).
[4] S. R. Leone, C. W. McCurdy, J. Burgdörfer, L. S. Cederbaum, Z. Chang, N. Dudovich, J. Feist, C. H. Greene, M. Ivanov, R. Kienberger, U. Keller, M. F. Kling, Z.-H. Loh, T. Pfeifer, A. N. Pfeiffer, R. Santra, K. Schafer, A. Stolow, U. Thumm, and M. J. J. Vrakking, Nat. Photonics **8**, 162 (2014).
[5] G. Sansone, F. Kelkensberg, J. F. Pérez-Torres, F. Morales, M. F. Kling, W. Siu, O. Ghafur, P. Johnsson, M. Swoboda, E. Benedetti, F. Ferrari, F. Lépine, J. L. Sanz-Vicario, S. Zherebtsov, I. Znakovskaya, A. L'Huillier, M. Y. Ivanov, M. Nisoli, F. Martín, and M. J. J. Vrakking, Nature (London) **465**, 763 (2010).
[6] F. Kelkensberg, W. Siu, J. F. Pérez-Torres, F. Morales, G. Gademann, A. Rouzée, P. Johnsson, M. Lucchini, F. Calegari, J. L. Sanz-Vicario, F. Martín, and M. J. J. Vrakking, Phys. Rev. Lett. **107**, 043002 (2011).
[7] G. Laurent, W. Cao, H. Li, Z. Wang, I. Ben-Itzhak, and C. L. Cocke, Phys. Rev. Lett. **109**, 083001 (2012).
[8] P. M. Paul, E. S. Toma, P. Breger, G. Mullot, F. Auge, P. Balcou, H. G. Muller, and P. Agostini, Science **292**, 1689 (2001).
[9] A. Jiménez Galán, L. Argenti, and F. Martín, New J. Phys. **15**, 113009 (2013).
[10] P. Agostini and L. F. DiMauro, Rep. Prog. Phys. **67**, 813 (2004).
[11] K. Klünder, J. M. Dahlström, M. Gisselbrecht, T. Fordell, M. Swoboda, D. Guénot, P. Johnsson, J. Caillat, J. Mauritsson, A. Maquet, R. Taïeb, and A. L'Huillier, Phys. Rev. Lett. **106**, 143002 (2011).
[12] D. Guénot, K. Klünder, C. L. Arnold, D. Kroon, J. M. Dahlström, M. Miranda, T. Fordell, M. Gisselbrecht, P. Johnsson, J. Mauritsson, E. Lindroth, A. Maquet, R. Taïeb, A. L'Huillier, and A. S. Kheifets, Phys. Rev. A **85**, 053424 (2012).
[13] J. M. Dahlström and E. Lindroth, J. Phys. B **47**, 124012 (2014).
[14] C. Hättig, W. Klopper, A. Köhn, and D. P. Tew, Chem. Rev. **112**, 4 (2012).
[15] F. Lépine, M. Y. Ivanov, and M. J. J. Vrakking, Nat. Photonics **8**, 195 (2014).
[16] J. Breidbach and L. S. Cederbaum, Phys. Rev. Lett. **94**, 033901 (2005).
[17] S. Pabst, L. Greenman, P. J. Ho, D. A. Mazziotti, and R. Santra, Phys. Rev. Lett. **106**, 053003 (2011).
[18] P. Ranitovic, X. M. Tong, B. Gramkow, S. De, B. DePaola, K. P. Singh, W. Cao, M. Magrakvelidze, D. Ray, I. Bocharova, H. Mashiko, A. Sandhu, E. Gagnon, M. M. Murnane, H. Kapteyn, I. Litvinyuk, and C. L. Cocke, New J. Phys. **12**, 013008 (2010).
[19] M. Swoboda, T. Fordell, K. Klünder, J. M. Dahlström, M. Miranda, C. Buth, K. J. Schafer, J. Mauritsson, A. L'Huillier, and M. Gisselbrecht, Phys. Rev. Lett. **104**, 103003 (2010).
[20] K. L. Ishikawa and K. Ueda, Phys. Rev. Lett. **108**, 033003 (2012).
[21] N. Shivaram, H. Timmers, X.-M. Tong, and A. Sandhu, Phys. Rev. Lett. **108**, 193002 (2012).
[22] N. Shivaram, H. Timmers, X.-M. Tong, and A. Sandhu, Chem. Phys. **414**, 139 (2013).
[23] P. Lambropoulos and P. Zoller, Phys. Rev. A **24**, 379 (1981).
[24] S. I. Themelis, P. Lambropoulos, and M. Meyer, J. Phys. B **37**, 4281 (2004).

[25] X. M. Tong and C. D. Lin, Phys. Rev. A **71**, 033406 (2005).
[26] Z. X. Zhao and C. D. Lin, Phys. Rev. A **71**, 060702 (2005).
[27] M. Wickenhauser, J. Burgdörfer, F. Krausz, and M. Drescher, J. Mod. Opt. **53**, 247 (2006).
[28] T. Morishita, S. Watanabe, and C. D. Lin, Phys. Rev. Lett. **98**, 083003 (2007).
[29] T. Sekikawa, T. Okamoto, E. Haraguchi, M. Yamashita, and T. Nakajima, Opt. Express **16**, 21922 (2008).
[30] L. Argenti and E. Lindroth, Phys. Rev. Lett. **105**, 053002 (2010).
[31] W.-C. Chu and C. D. Lin, Phys. Rev. A **82**, 053415 (2010).
[32] W.-C. Chu, S.-F. Zhao, and C. D. Lin, Phys. Rev. A **84**, 033426 (2011).
[33] W.-C. Chu and C. D. Lin, Phys. Rev. A **85**, 013409 (2012).
[34] L. Argenti, R. Pazourek, J. Feist, S. Nagele, M. Liertzer, E. Persson, J. Burgdörfer, and E. Lindroth, Phys. Rev. A **87**, 053405 (2013).
[35] W.-C. Chu, T. Morishita, and C. D. Lin, Phys. Rev. A **89**, 033427 (2014).
[36] J. Caillat, A. Maquet, S. Haessler, B. Fabre, T. Ruchon, P. Salières, Y. Mairesse, and R. Taïeb, Phys. Rev. Lett. **106**, 093002 (2011).
[37] E. Lindroth and L. Argenti, Adv. Quantum Chem. **63**, 247 (2012).
[38] U. Fano, Phys. Rev. **124**, 1866 (1961).
[39] R. Madden and K. Codling, Phys. Rev. Lett. **10**, 516 (1963).
[40] J. Cooper, U. Fano, and F. Prats, Phys. Rev. Lett. **10**, 518 (1963).
[41] G. Tanner, K. Richter, and J.-M. Rost, Rev. Mod. Phys. **72**, 497 (2000).
[42] See Supplemental Material at http://link.aps.org/supplemental/10.1103/PhysRevLett.113.263001 for outline of the model derivation, calibration and robustness test.
[43] M. Abramowitz and I. A. Stegun, *Handbook of Mathematical Functions with Formulas, Graphs, and Mathematical Tables* (Dover, New York, 1965).
[44] V. Véniard, R. Taïeb, and A. Maquet, Phys. Rev. A **54**, 721 (1996).
[45] P. Saliéres (private communication).
[46] J. Mauritsson, T. Remetter, M. Swoboda, K. Klünder, A. L'Huillier, K. J. Schafer, O. Ghafur, F. Kelkensberg, W. Siu, P. Johnsson, M. J. J. Vrakking, I. Znakovskaya, T. Uphues, S. Zherebtsov, M. F. Kling, F. Lépine, E. Benedetti, F. Ferrari, G. Sansone, and M. Nisoli, Phys. Rev. Lett. **105**, 053001 (2010).